frontiers in Mechanical Engineering

ORIGINAL RESEARCH
published: 15 February 2021
doi: 10.3389/fmech.2020.629243

The Influence of Charge Motion on Pre-Chamber and Main Chamber Combustion in a Highly Dilute Jet Ignition Engine

Michael Bunce[1,2]*, *Alasdair Cairns*[1], *Sai Krishna Pothuraju Subramanyam*[2], *Nathan Peters*[2] *and Hugh Blaxill*[2]

[1]Department of Mechanical, Materials and Manufacturing Engineering, University of Nottingham, Nottingham, United Kingdom, [2]MAHLE Powertrain LLC, Plymouth, MI, United States

Though there are multiple viable powertrain options available for the automotive sector, those that contain internal combustion engines will continue to account for the majority of global sales for the next several decades. It is therefore imperative to continue the pursuit of novel combustion concepts that produce efficiency levels significantly higher than those of current engines. Introducing high levels of dilution in spark ignited (SI) engines has consistently proven to produce an efficiency benefit compared to conventional stoichiometric engine operation. However, this combustion mode can present challenges for the ignition system. Pre-chamber jet ignition enables stable, highly dilute combustion by both increasing the ignition energy present in the system and distributing it throughout the combustion chamber. Previous work by the authors have shown that jet ignition produces 15–25% increases in thermal efficiency over baseline SI engines with only relatively minor changes to engine architecture. Lean combustion in general and jet ignition in particular represent fundamentally different engine operating modes compared to those of conventional stoichiometric SI engines. Therefore, there are some system sensitivities not present in stoichiometric engines that must be investigated in order to fully optimize the jet ignition system. Differing types and magnitudes of charge motion are incorporated in SI engines to aid with mixture preparation but the influence of charge motion over lean combustion performance, particularly in jet ignition engines, is less well understood. This study analyzes the impact that charge motion has on both pre-chamber and main chamber combustion. A 1.5 L 3-cylinder gasoline engine is outfitted with multiple intake port configurations producing varying magnitudes and types of charge motion. Pre-chamber and main chamber combustion stability and other burn parameter responses are analyzed across multiple speeds and loads, including at critical operating points such as a catalyst heating condition. The results show that there is combustion sensitivity to charge motion, resulting in >1 percentage point spread in peak thermal efficiency for the configurations tested, and that this sensitivity manifests most significantly under low ignitability conditions such as heavy dilution. These results provide guidance for future system optimization of jet ignition engines.

Keywords: pre-chamber, jet ignition, dilution, lean combustion, charge motion

OPEN ACCESS

Edited by:
Yuanjiang Pei,
Aramco Services Company,
United States

Reviewed by:
Xin Yu,
Aramco Services Company,
United States
Toby Rockstroh,
Argonne National Laboratory (DOE),
United States
Jean-Marc Zaccardi,
IFP Energies nouvelles (IFPEN), France

***Correspondence:**
Michael Bunce
mike.bunce@mahle.com

Specialty section:
This article was submitted to Engine and Automotive Engineering, a section of the journal Frontiers in Mechanical Engineering

Received: *13 November 2020*
Accepted: *30 December 2020*
Published: *15 February 2021*

Citation:
Bunce M, Cairns A, Krishna Pothuraju Subramanyam S, Peters N and Blaxill H (2021) The Influence of Charge Motion on Pre-Chamber and Main Chamber Combustion in a Highly Dilute Jet Ignition Engine. Front. Mech. Eng 6:629243. doi: 10.3389/fmech.2020.629243

INTRODUCTION

Increasingly stringent global legislation of greenhouse gas emissions from the transportation sector requires a step change in internal combustion engine (ICE) efficiency. A method being explored to accomplish this goal is dilute gasoline combustion (Bunce et al., 2014; Bunce and Blaxill, 2016). A major limitation in developing dilute combustion systems is the less favourable ignition quality of the mixture. This has necessitated the development of higher energy ignition sources (Quader, 1974; Yamamoto, 1999). A pre-chamber combustor is one such technology (Germane et al., 1983; Heywood, 1988; Husted et al., 2009). Pre-chamber combustion concepts have demonstrated the potential for stable main chamber combustion at high levels of dilution (Attard et al., 2010).

SI engines that utilize pre-chambers generally retain the spark plug but relocate it to the pre-chamber and repurpose it as the ignition source for the air-fuel charge present in the pre-chamber. Products from this combustion event are then transferred to the main chamber through an orifice(s) or valve, thermo-chemically igniting the main chamber air-fuel charge (Biswas et al., 2016; Mastorakos et al., 2017). This provides greater ignition energy compared to that of a standard single-point spark plug. This leads to burn durations with pre-chamber combustors approximately 30–50% quicker than those of conventional spark ignition engines at similar conditions.

Pre-chamber combustion concepts have demonstrated the potential for stable main chamber combustion at higher levels of dilution than are allowable in typical SI engines (Attard et al., 2010; Bureshaid et al., 2019). They have also demonstrated the ability to counter the loss of ignitability of lean air-fuel charge. This capability results in an extension of the lean limit of the engine. As the air-fuel charge is enleaned, the portion of this charge entering the pre-chamber becomes regressively ignitable with a standard spark plug. Auxiliary fueling in the pre-chamber can compensate for the enleanment of this incoming charge, extending the lean limit further and enabling the engine to operate in an ultra-lean (lambda > 1.6) combustion mode. Direct injection (DI) fuel injector technology has removed one of the major technological barriers and renewed interest in this concept (Toulson et al., 2010), as have modern machining techniques that enable smaller pre-chamber volumes than were previously allowable.

MAHLE Powertrain has been developing a pre-chamber combustor concept known as MAHLE Jet Ignition (MJI)® since 2009 (Bunce et al., 2014; Chinnathambi et al., 2015; Bunce and Blaxill, 2016). The use of a micro-flow DI fuel injector in the MJI pre-chamber allows for precise, consistent metering of small quantities of fuel each cycle and precise targeting of the fuel spray. The high-pressure capabilities of modern DI fuel injection systems also enable relatively late fuel injection in the pre-chamber which in turn allows the fuel strategy to exploit the local charge motion interior to the pre-chamber during the compression stroke. This innovation to the jet ignition concept is viewed as critical for 1) successful operation with a liquid pre-chamber fuel, and 2) efficient, judicious use of the pre-chamber fuel in order to ensure a strong system efficiency increase. The MJI pre-chamber prototype assembly is displayed in **Figure 1**.

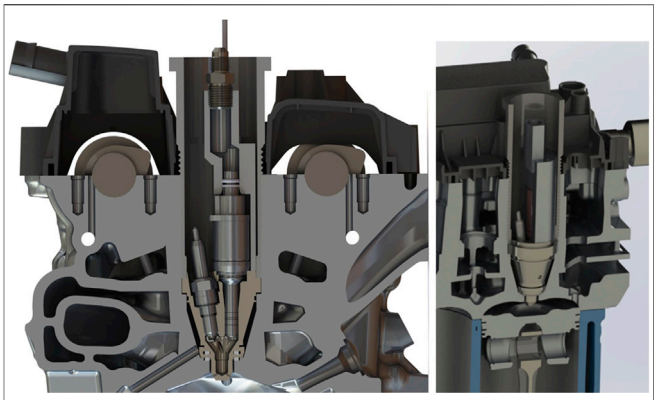

FIGURE 1 | Cutaway of the MJI pre-chamber **(left)** and MJI pre-chamber assembly **(right)** in a typical passenger car engine cylinder head.

MJI incorporates the characteristics of many jet ignition concepts researched since the early 1990s, namely a small volume pre-chamber (<5% of the clearance volume) and a multi-orifice nozzle with orifice diameters that promote a high degree of flame quenching. These characteristics are common to both passive (no auxiliary fueling) and active (auxiliary fueled) jet ignition variants. The quenching and re-ignition process was confirmed through images taken from an optically accessible engine, shown in **Figure 2**. The images in this figure show luminous jets, with no backlighting, emerging from the pre-chamber. The flame content in these jets is minimal. The jets subsequently create distinct ignition sites in the main chamber, visible at the leading edges of the jets, particularly in the bottom row of images. These ignition sites produce distinct flame fronts that consume the charge, eventually joining during this process. More details of this study are provided in (Bunce et al., 2014).

Peak brake thermal efficiency (BTE) published to-date in an MJI engine is 42% (Bunce and Blaxill, 2016), representing an increase of approximately 20% over the baseline SI version of the engine, and 10% above the highest reported production-intent SI engine BTE at the time of this writing. A subsequent MJI engine study in review has demonstrated a peak BTE >43.5% and a minimum brake specific fuel consumption (BSFC) < 190 g/kWh with the use of advanced lubricants and gasoline-range fuels (Society of Automotive Engineers manuscript submission entitled: "The Impact of Advanced Fuels and Lubricants on Thermal Efficiency in a Highly Dilute Engine").

Jet ignition concepts generally and MJI specifically possess numerous parameters than can be optimized in order to increase BTE, minimize engine-out emissions, or aid practical engine operation. While many of these parameters have been studied extensively by the authors (Bunce et al., 2014) and others (Gussak et al., 1979; Dale and Oppenheim, 1981; Wakai et al., 1993; Murase and Hanada, 2000; Biswas et al., 2016; Mastorakos et al., 2017), one parameter for which there is minimal published data on its effect on jet ignition combustion processes is charge motion.

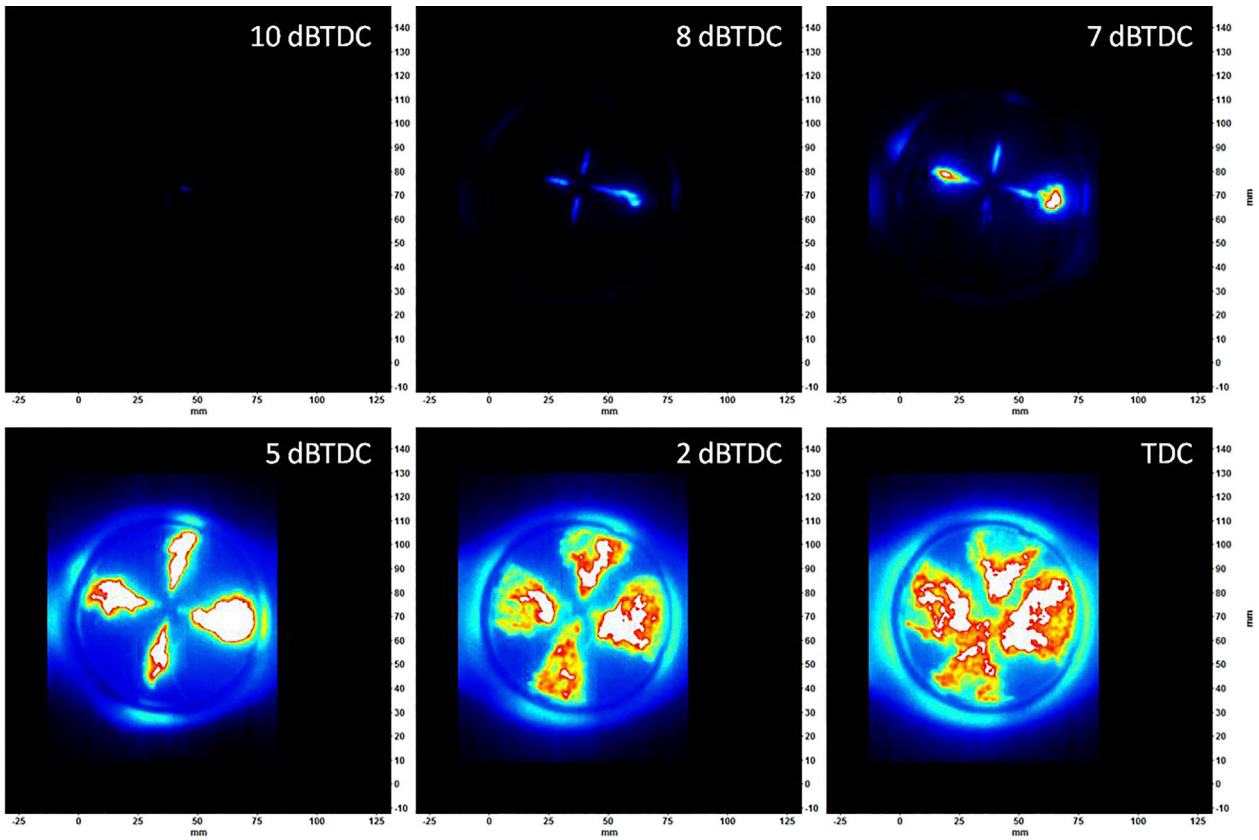

FIGURE 2 | Chemiluminescence high speed images of the jet ignition process (Speed: 1,500 rpm, gross indicated mean effiective pressure (IMEPg): 5.5 bar, lambda = 1.2) taken from an optically accessible engine. See Bunce et al., (2014) for more details of this study.

Charge motion in SI engines is typically used to drive or enhance mixture preparation in the cylinder. With the advent of DI SI engines, the role of charge motion in mixture preparation has become especially critical to ensuring successful combustion and low emissions. The pervasive type of charge motion used in SI engines is tumble, which typically interacts with the bulk of the injector spray. Tumble requires certain length scales and tends to degrade as the piston nears top-dead center (TDC) (Qi et al., 2015; Ruhland et al., 2017; Bozza et al., 2018), though this effect is highly dependent on combustion chamber geometry, especially compression ratio and stroke-to-bore ratio. It devolves into a general non-ordered turbulent kinetic energy (TKE) with high velocity but no uniform flow field. As such tumble motion tends to not contribute strongly to combustion in and of itself, but high levels of TKE present during the combustion process can increase turbulent flame speed, thereby increasing combustion burn rate. This effect is particularly useful for lean engines, as it helps compensate for the reduction in laminar flame speed inherent in the colder lean combustion environment. High levels of turbulence can, however, have the detrimental effect of stretching the spark kernel, resulting in misfires, and also increase in-cylinder heat loss.

Swirl motion is generally not purposefully used in production SI engines as it provides little mixture preparation benefit. It does not degrade near TDC to nearly the same extent as tumble and therefore it is a potentially useful form of charge motion for lean combustion concepts as it exists during the combustion process. Literature (Hill and Zhang, 1994; Patrie et al., 1998; Loeper et al., 2014) and previous simulations performed by MAHLE Powertrain have shown contradictory effects of swirl on lean combustion.

Quader (et al.) demonstrated that charge motion has a competing influence on kernel formation and flame front propagation in homogeneous lean combustion SI engines (Quader, 1974; Peters and Quader, 1978). High levels of charge motion, regardless of type, can have the effect of stretching the flame kernel resulting in misfires. Contrarily, high levels of charge motion prove beneficial to increasing flame speed as the flame slowly consumes the lean charge. Stratified lean combustion with targeted mixture preparation to ensure an ignitable mixture near the spark plug is one potential solution that has been proposed to mitigate the kernel formation challenge of high tumble dilute engines (Urushihara et al., 1996; Solomon and Szekely, 2003). Alternatively, pre-chamber concepts have the potential to effectively separate and quarantine the spark plug from the majority of the main combustion chamber flow field. This could potentially lead to high levels of TKE in the main chamber being beneficial to reducing burn duration and

increasing enleanment while reducing the risk of kernel stretching. While flow into the pre-chamber during the compression stroke can produce a high velocity charge column, careful pre-chamber design can minimize the impact of this flow on kernel formation.

Historically jet ignition concepts have had limited success achieving acceptable combustion stability under low load operation including idle and catalyst heating operation (Vedula et al., 2017; Sens et al., 2018). These conditions require a high degree of spark retard capability, a capability that is typically lacking with jet ignition concepts. Catalysts require heat input to work effectively. Prior to achieving a high temperature light-off condition a large proportion of the engine-out emissions pass through un-catalyzed or uncaptured to the tailpipe. Aggressive warm up of the catalysts is therefore critical to ensuring that the vehicle can meet legislated emissions requirements. The common solution to ensure rapid heat input to the catalyst is to retard spark timing to such a degree that combustion occurs exclusively during the expansion stroke. The much later burning process results in both increased exhaust temperature and increased exhaust flow, the latter due to the de-throttling necessary to maintain a modest engine load under highly inefficient conditions. The combined increases in exhaust temperature and flow produce a relatively high exhaust enthalpy at this condition. Spark retard, and its ability to generate high exhaust enthalpy, therefore is an essential element of catalyst heating operation, which makes pre-chambers' nominal lack thereof a major concern. A previous study by the authors demonstrated the ability of MJI to overcome the traditional pre-chamber spark retard limitation (Bunce et al., 2019). However, the impact that charge motion level and type have on MJI spark retard capability is unknown.

This study seeks to understand the impact of charge motion level and type on jet ignition combustion performance and to quantify the thermal efficiency potential of optimized charge motion in a jet ignition engine. This study also seeks to quantify the sensitivity of catalyst heating performance to charge motion level and type.

MATERIALS AND METHODS

Experimental Apparatus

The jet ignition engine used as the research platform in the present study is an in-line turbocharged 3-cylinder based on the 1.2 L MAHLE DI3 Downsizing demonstrator whose development has been well documented (Bassett et al., 2017). The stroke has been elongated to increase the displacement to 1.5 L. It is able to be converted to either DI or port fuel injection (PFI) for the main chamber fueling and is used in the PFI configuration for this study. The compression ratio (CR) used in this study is 15:1, slightly higher than the typical 14:1 CR used in previous studies. This was done in order to ensure that the engine would achieve knocking conditions under lean operation so that charge motion sensitivity under non-knock-limited conditions could be compared with that under knock-limited conditions. Engine specifications are listed in **Table 1** and the engine and test cell schematic are depicted in **Figure 3**.

TABLE 1 | Engine specifications.

Parameter	Description
Configuration	In-line 3 cylinder
Displaced volume	1,500 cm^3
Stroke	92.4 mm
Bore	83 mm
Compression ratio	15:1 for this study
Piston crown	Flat top with valve cutouts
Number of valves	4
Injection	PFI main chamber, DI pre-chamber
Fuel	Pump grade premium gasoline
Number of pre-chamber orifices	6
Pre-chamber volume	1.0 cm^3
Cylinder head geometry	Pent-roof with offset pre-chamber
Boost system	Variable-geometry turbocharger

The engine incorporates an identical pre-chamber assembly into each cylinder. The pre-chamber assembly houses a fuel injector, spark plug, and high-speed pressure transducer (main chamber—Kistler 6041, pre-chamber – AVL GH14). The pre-chamber body and nozzle are separate pieces to allow for the use of interchangeable hardware. Pre-chamber and nozzle geometric specifications were determined using patented relationships (Bunce and Blaxill, 2018) developed as part of previous projects.

Engine speed is controlled by a motoring dynamometer. At each operating condition, the engine control unit (ECU) varies throttle position and main chamber fuel quantity to achieve a commanded brake mean effective pressure (BMEP) at the commanded overall lambda in a closed loop mode. Commanded lambda is controlled via a wide-band oxygen (O_2) sensor located in the exhaust manifold. This sensor reading is verified with a calculated lambda from measured exhaust emissions and from air flow and fuel flow measurements. Exhaust emissions are measured using an AVL AMA i60 emissions bench that contains carbon dioxide (CO_2), carbon monoxide (CO), total hydrocarbons (THC), methane (CH_4), O_2, and nitrogen oxides (NO_x) analyzers. As the engine is enleaned beyond lambda = 1.3, the pulsewidth of the pre-chamber DI is increased to maintain the coefficient of variation (COV) of gross indicated mean effective pressure (IMEPg) less than 3%. Main chamber and pre-chamber fuel flow rates are measured using a MicroMotion Coriolis flow meter and Bronkhorst M13 Coriolis flow meter, respectively. Unless otherwise stated all efficiency and fuel consumption metrics are calculated using total fuel flow to both chambers.

Both main chamber PFI and pre-chamber auxiliary DI fuel pressure are provided externally in the test cell and are nominally set to 4 and 100 bar, respectively. The friction penalty for operating a fuel pump to feed the high pressure pre-chamber DI is small due to the low fuel flow rate used by the pre-chamber. Using a fuel pressure of 100 bar with a conservative fuel pump efficiency of 60%, the resulting impact on the brake efficiency values presented here would be less than 0.1%. This friction penalty is disregarded for the purposes of this study.

Data quality was monitored using a series of daily check points that spanned stoichiometric non-auxiliary fueled operation and

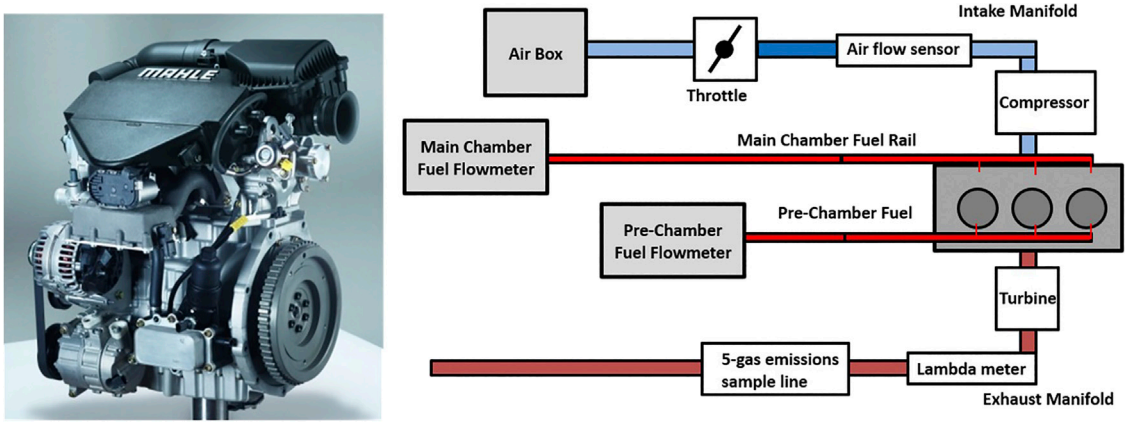

FIGURE 3 | DI3 engine **(left)** and schematic of the testing setup **(right)**.

lean auxiliary fueled operation. At these daily check points, fuel injector pulsewidth, throttle position, and spark timing were fixed. A moving average of ±5% of the following parameters was deemed an acceptable range of variation: IMEPg, indicated thermal efficiency (ITE), crank angle duration of 10–90% fuel mass burned (CA10-90), angle of 50% fuel mass burned (CA50), friction mean effective pressure (FMEP), COV, fuel flow rate (main chamber and pre-chamber), lambda, and NO_x. If any of these parameters exceeded the ±5% threshold, the source of error was identified and rectified, and the daily check point was re-recorded.

Low speed data was recorded and averaged over a 30 s interval. Three of these 30 s intervals were recorded and averaged consecutively, and the three averages were averaged again. These three averages were evaluated for consistency. High speed pressure data was acquired from each of the three main chambers and pre-chambers, and the intake port of one cylinder, with the log beginning simultaneous to the start of the low speed data log. High speed data was acquired for 300 consecutive cycles and then averaged.

An Air Flow Rig was used to evaluate tumble ratio and swirl number of several charge motion variants of the engine. The Air Flow Rig forces air to flow through the cylinder head, while valve lift is adjusted statically in 1 mm increments. Tumble ratio and swirl number are calculated by integrating the area under the resulting non-dimensional tumble vs. lift and swirl vs. lift curves, respectively.

Four charge motion cases were evaluated: baseline, increased tumble, introduction of swirl, and a combination of swirl and tumble (denoted as "swumble" in subsequent sections). Charge motion differences from the baseline were induced through the use of plate inserts into each of the intake ports (**Figure 4**). The baseline configuration used no inserts and represents a moderate tumble engine consistent with tumble levels in modern DI SI engines (a tumble ratio of approximately 3). For the tumble variant, a plate insert was used that directed flow to exit past the valve in a more severe tumble motion. For the swirl variant, a splitter plate was used with a slight incline across the diameter of the port to induce swirl. The swumble variant used the swirl plate and tumble plate in series. The relative change in tumble ratio and swirl number with respect to the baseline (no inserts) port are listed in **Table 2**.

Methodology

The engine was used to experimentally quantify the impact of charge motion on performance by comparing data using all 4 charge motion variants. Three categories of operating condition were investigated:

(1) Non-knock-limited operation–a speed/load condition that does not exhibit any knock tendency under lean conditions
(2) Knock-limited operation–a speed/load condition that does exhibit a tendency to knock under lean conditions and therefore requires spark retard to avoid knock
(3) Cold start spark retard (CSSR) operation–a speed/load condition consistent with the catalyst light-off conditions of modern production engines.

For conditions 1 and 2, lambda sweeps were performed, whereby speed and load were held constant as the lambda of the engine was increased from 1.0 to its lean limit in increments of 0.1. The lean limit defined in these tests is the lambda at which consistent detectable misfires prevent the engine from holding its proscribed operating conditions, or the point at which the boost system of the engine is incapable of providing enough airflow to maintain the desired load.

For condition 1, BMEP was used as the constant load parameter due to the reduced influence of pumping losses for a non-boosted condition that achieves wide open throttle when lean. For condition 2, IMEPg is used as the constant load parameter due to the significant influence of pumping losses associated with heavy boosting.

For both conditions, the pre-chamber fuel injector is used to provide auxiliary fuel when the engine achieves a lambda = 1.4. As the engine is enleaned, the pre-chamber fueling quantity is increased. With all charge motion variants, the pre-chamber auxiliary fuel is kept to the minimum allowable value to maintain COV < 3%. The baseline and tumble variants

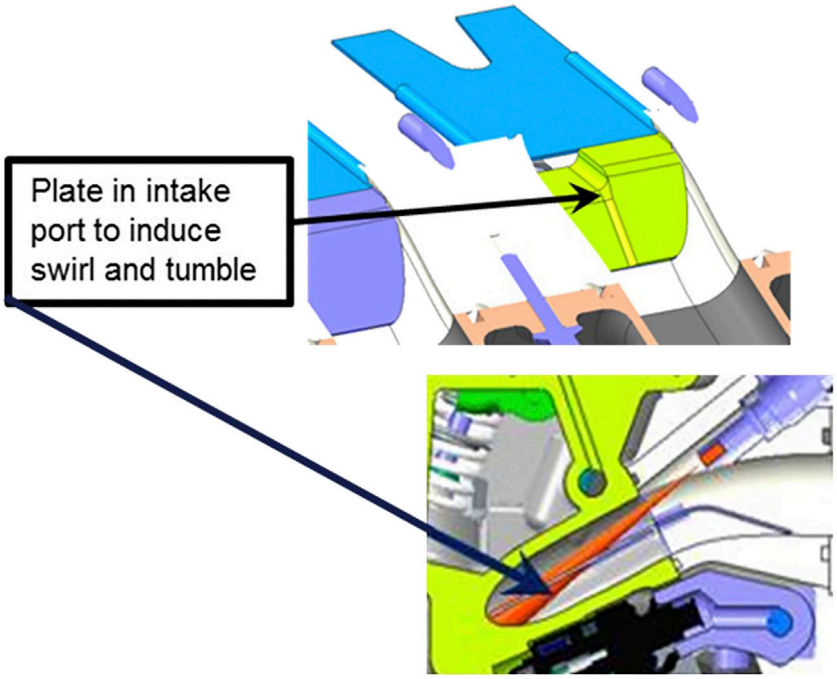

FIGURE 4 | Illustration of tumble plate insert in 1.5 L jet ignition engine.

TABLE 2 | Relative change in tumble ratio and swirl number with various intake port insert configurations, relative to the baseline configuration.

Configuration	Relative tumble ratio (%)	Relative swirl number (%)
Baseline	—	—
Tumble	+13	−25
Swirl	−39	+1,075
Swirl+Tumble	+13	+75

utilized nearly identical quantities of auxiliary fuel vs. lambda, while the swirl and swumble variants generally required approximately double this quantity at the leanest conditions tested (lambda > 1.8). For all variants across all data points, the maximum fuel mass injected using the pre-chamber fuel injector was approximately 1.5% of the fuel mass injected through the main chamber fuel injector.

For the knock limited condition 2, CA50 was advanced at each lambda point with each charge motion variant until the engine achieved a previously established speed-sensitive knock amplitude threshold as calculated from the main chamber high speed pressure transducers that represented a no/light knock condition. These results were confirmed qualitatively in real-time using an acoustic knock tube. No knock or pre-ignition was detected in the pre-chambers, which is consistent with the results of other tests of this engine/pre-chamber configuration.

Conditions 1 and 2 operated with approximately 60 degrees of valve overlap, which was determined to be optimal for thermal efficiency at these conditions. Condition 1 achieved wide open throttle near the lean limit of the engine, with only mild boost being employed throughout the testing at this condition. Condition 2 achieved wide open throttle in the near-lean region, with a maximum boost pressure of approximately 1.5 bar near the lean limit. At both conditions, back pressure was applied via a back pressure valve in order to mimic the effect of a catalyst. The use of the back pressure valve ensured a negative delta pressure across the engine at all conditions.

For condition 3, a sweep of spark timing was performed at a constant speed, load, and lambda with fluids chilled to 25°C in order to emulate a CSSR catalyst heating condition. The specified speed and load are consistent with CSSR conditions for modern production engines. Net indicated mean effective pressure (NMEP) was held as the constant load parameter due to the reduced disparity in pumping losses among the charge motion variants at this condition, and for the traditional specification of NMEP as the relevant load for CSSR conditions. A slightly lean lambda was selected using criteria established in a previous study of CSSR jet ignition operation, detailed in (Bunce et al., 2019).

Pre-chamber combustion was analyzed through the use of high speed pressure transducers located in the pre-chambers. Data from these transducers were paired with the corresponding main chamber in-cylinder pressure transducers to provide a clear perspective on intra-chamber pressure-based behavior. For this study, high speed pre-chamber and main chamber results from one of the three cylinders are presented in order to avoid the use of corrections for minor cylinder-to-cylinder differences. Each presented high speed data point represents an analysis of 300

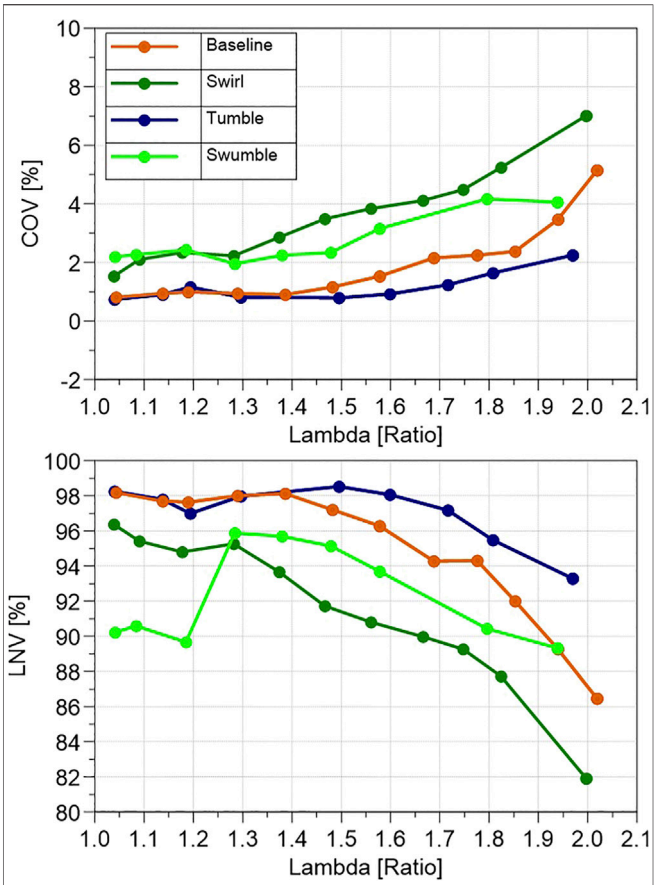

FIGURE 5 | Combustion stability metrics vs. lambda; 1,500 rpm, 6 bar BMEP, angle of 50% fuel mass burned (CA50) = 8° after TDC.

consecutive cycles. The methodology used to analyze these results, and the relative importance of the calculated metrics are described in detail in (Peters et al., 2020).

RESULTS

Non-Knock Limited Operation

Jet ignition engine sensitivity to charge motion is first examined at condition 1, a non-knock limited part load condition (1,500 rpm, 6 bar BMEP). Results are presented across a sweep of lambda, from 1.0 to the lean limit of the engine at this condition. Knock is not prevalent for any of the charge motion variants except at the lambda values closest to 1.0. **Figure 5** shows the two relevant combustion stability metrics, COV and lowest normalized value of IMEPg (LNV). Modern production ICEs typically hold to a COV limit ≤3%. An LNV value <88% indicates a high likelihood that a partial burn event has occurred, whereby a significant portion of the fuel present in the cylinder is not consumed by the combustion flame in multiple intermittent cycles.

In **Figure 5**, it is evident that the tumble variant maintains acceptable stability throughout the range of lambda from 1.0 to 2.0, without any partial burn events. The baseline variant performs similarly but with increased instability from lambda 1.5 and a stability limit from lambda 1.9. There is also more pronounced deterioration in LNV in this lean lambda range. The swirl and swumble variants perform measurably poorer, with stability limits reached between lambda 1.3 and 1.4.

Figure 6 shows the CA50 for the charge variants, confirming that light knock may be present near lambda 1.0 but it is absent for all variants from lambda 1.2. The instability in CA50 in the near-lean region (lambda = 1.0–1.3) is due to cylinder-to-cylinder variation that manifests under lean conditions but is mitigated by the addition of pre-chamber auxiliary fuel starting at lambda = 1.4. An examination of the burn duration segments shows that the two variants that include increased tumble motion (tumble and swumble variants) produce faster overall combustion duration. The difference in burn duration among the variants becomes prominent under lean conditions, with minimal separation at lambda 1.0. Under lean conditions, the swirl variant exhibits consistently slower late burning (CA50-90) than the other variants.

The burn duration results translate well to the combustion efficiency trends depicted in **Figure 7**. While combustion efficiency reduces with increasing enleanment, the swirl variant produces depressed combustion efficiency vs. the other charge motion variants across the lambda range starting from lambda 1.2. With late burning performance having a prominent impact on combustion efficiency, this swirl variant performance is expected. Conversely, the tumble variant produces the highest relative combustion efficiencies under lean conditions. Note that the combustion efficiencies depicted in **Figure 7**, especially under lean conditions, are lower than would be expected for this type of combustion system. This is due to the relatively high CR for an SI engine coupled with the homogeneous mixture leading to a relatively greater crevice volume fuel percentage of total fuel than would be found in production engines. Also note that the piston and ring combination used for this study are not production-intent and are not based on any existing production designs, and are therefore not optimized for the purposes of this combustion system.

While not directly related in traditional stoichiometric ICEs, combustion efficiency has some influence over thermal efficiency under lean conditions. The competing efficiency pathways of reduced in-cylinder heat losses and increased incomplete combustion losses (the latter captured in the combustion efficiency metric) with enleanment result in a lambda that corresponds to peak thermal efficiency occurring at a richer lambda than the lean limit. This effect is present in these results as well, with the peak BTE lambda occurring approximately between lambda 1.6 and 1.7 for most variants. Because BMEP was held constant among the charge motion variants at this speed/load condition, BTE provides the most accurate comparison. Here the results largely mirror the stability, burn duration, and combustion efficiency trends, with the tumble variant producing the highest BTE, followed by the baseline, swumble, and swirl variants, with the latter exhibiting rapid deterioration in BTE beyond the lean stability limit. ITE, which does not consider the relative pumping losses

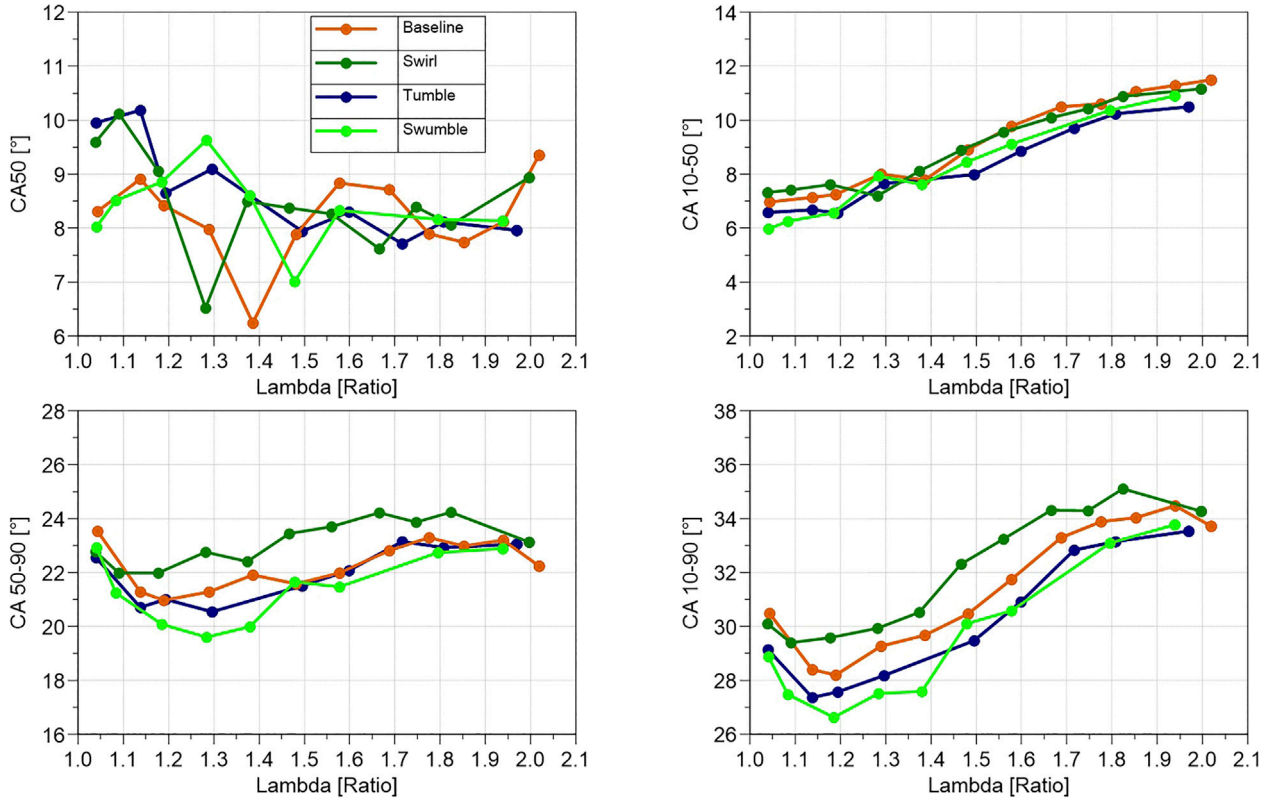

FIGURE 6 | Burn duration metrics vs. lambda; 1,500 rpm, 6 bar BMEP.

encountered across the lambda sweep at this condition, exhibits similar trends but with differing peak efficiency lambda values.

It is not known why the swirl variant outperforms the swumble variant in both BTE and ITE in the range of lambda = 1.4–1.7 despite this trend not being reflected in either the burn duration or combustion efficiency metrics. This could be due to minor discrepancies in load among the variants in this range.

Analysis of brake specific NO_x emissions trends vs. lambda in **Figure 7** show relative parity among the charge motion variants from lambda = 1.0–1.6. The erratic trends in the range beyond lambda = 1.6 do not appear to mirror any other major parameter's trend, and are likely the result of unstable combustion, particularly in the swirl and swumble variant data. Therefore, it does not appear that charge motion has any noticeable impact on NO_x formation at this condition. However, the comparison of **Figures 5** and **7** demonstrates the benefit of enhanced combustion stability in the ultra-lean region, namely the ability to further reduce NO_x emissions by operating at stably leaner lambda values.

An efficiency loss analysis is presented in **Figure 8** for the charge motion variants at lambda = 1.0 and 1.8. At the lambda = 1.0 condition, pumping work was corrected to account for the restriction of the plate inserts in the charge motion variants; such a correction was not needed at the lambda = 1.8 condition due to reduced relative significance of pump work. At both lambda values, the tumble variant displays slightly increased in-cylinder heat loss compared with the baseline, with the swirl and swumble variants exhibiting the highest in-cylinder heat loss. Also, notably at both lambda conditions the swirl variant produces the highest incomplete combustion loss, consistent with the CA50-90 trends.

Figure 9 shows an analysis of pre-chamber combustion data, providing an indication of the influence of charge motion on in-pre-chamber behavior. The parameter with the most prominent correlation with main chamber COV is the chamber delta pressure. As illustrated in the top left image of **Figure 9**, chamber delta pressure is the largest measured difference in pre-chamber and main chamber pressure. This delta is maximized during the pre-chamber combustion event, approximately midway through the pressure rise event in the pre-chamber. Previous research has shown that this point generally corresponds with the angle at which reactive jets first emerge from the pre-chamber. While the magnitude of chamber delta pressure does vary somewhat among the four charge motion variants, the standard deviation of chamber delta pressure provides perhaps the most robust indication of pre-chamber combustion stability (Bunce et al., 2019). The upper right plot shows the correlation between the standard deviation of chamber delta pressure and main chamber COV for the data points analyzed (data for all four charge motion variants at lambda = 1.0, 1.4, and 1.8). The correlation is particularly robust at the leanest conditions analyzed, as evidenced by the lower

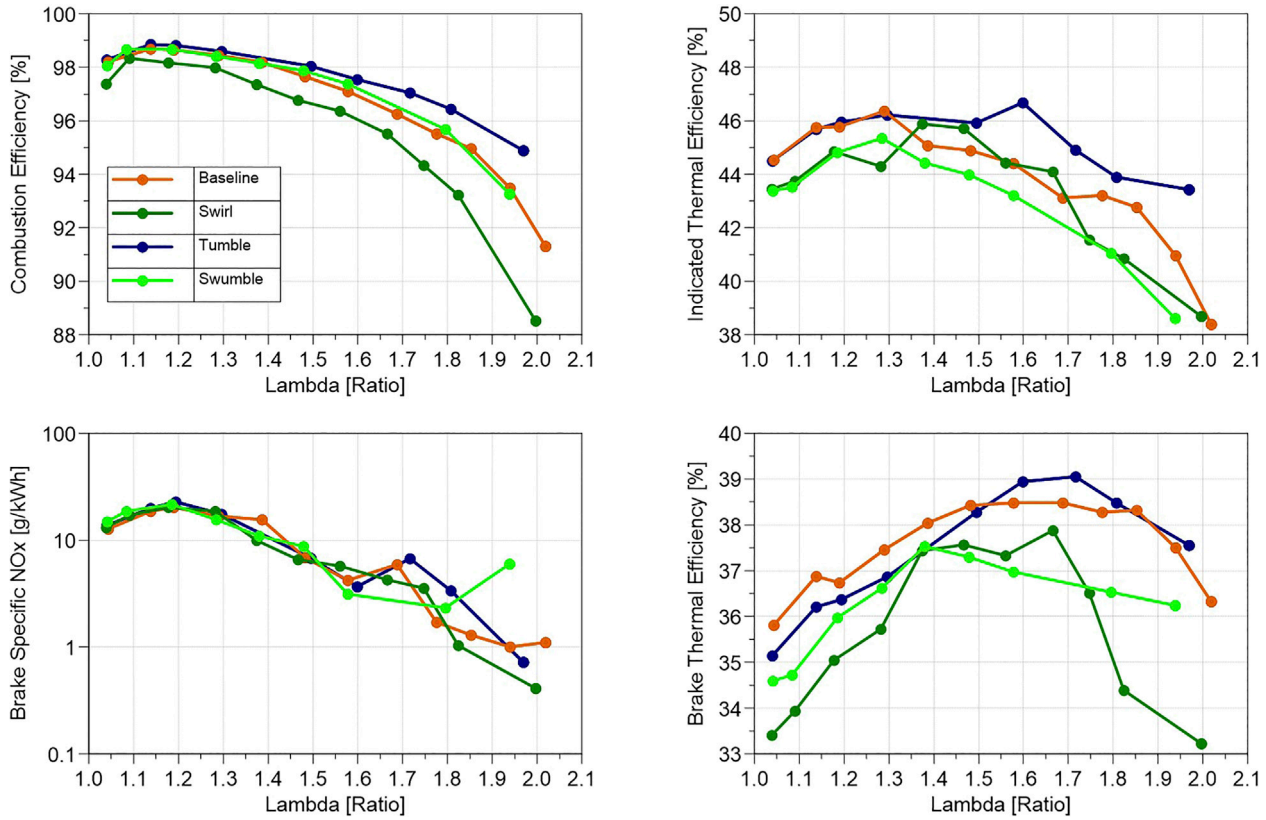

FIGURE 7 | Efficiency and emissions metrics vs. lambda; 1,500 rpm, 6 bar BMEP, CA50 = approximately 8° after TDC.

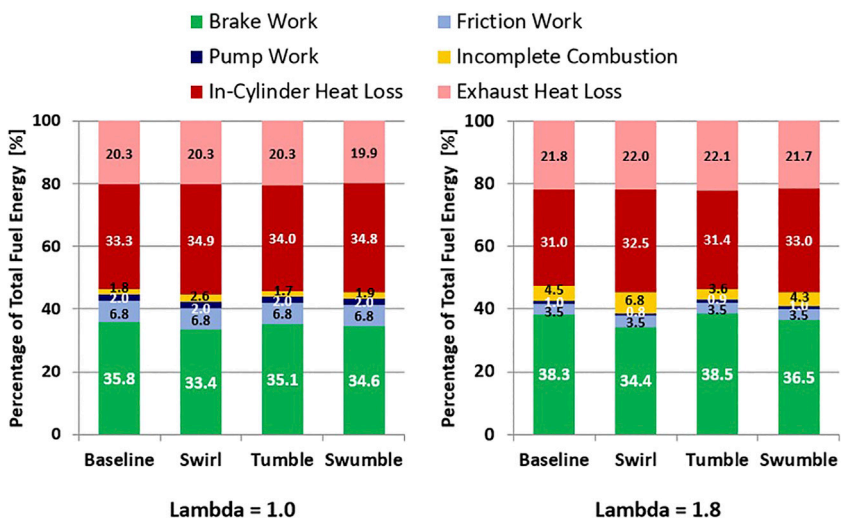

FIGURE 8 | Efficiency loss analysis as a percentage of total fuel energy; 1,500 rpm, 6 bar BMEP, lambda = 1.0 **(left)** and lambda = 1.8 **(right)**.

right plot. Practically, this means that the variation in the peak pressure generated in the pre-chamber by the pre-chamber combustion event induces variation in main chamber combustion performance.

The lower left plot in **Figure 9** shows the difference in standard deviation of chamber delta pressure among the four charge motion variants. Notably, these results mirror both the main chamber COV and combustion efficiency trends discussed

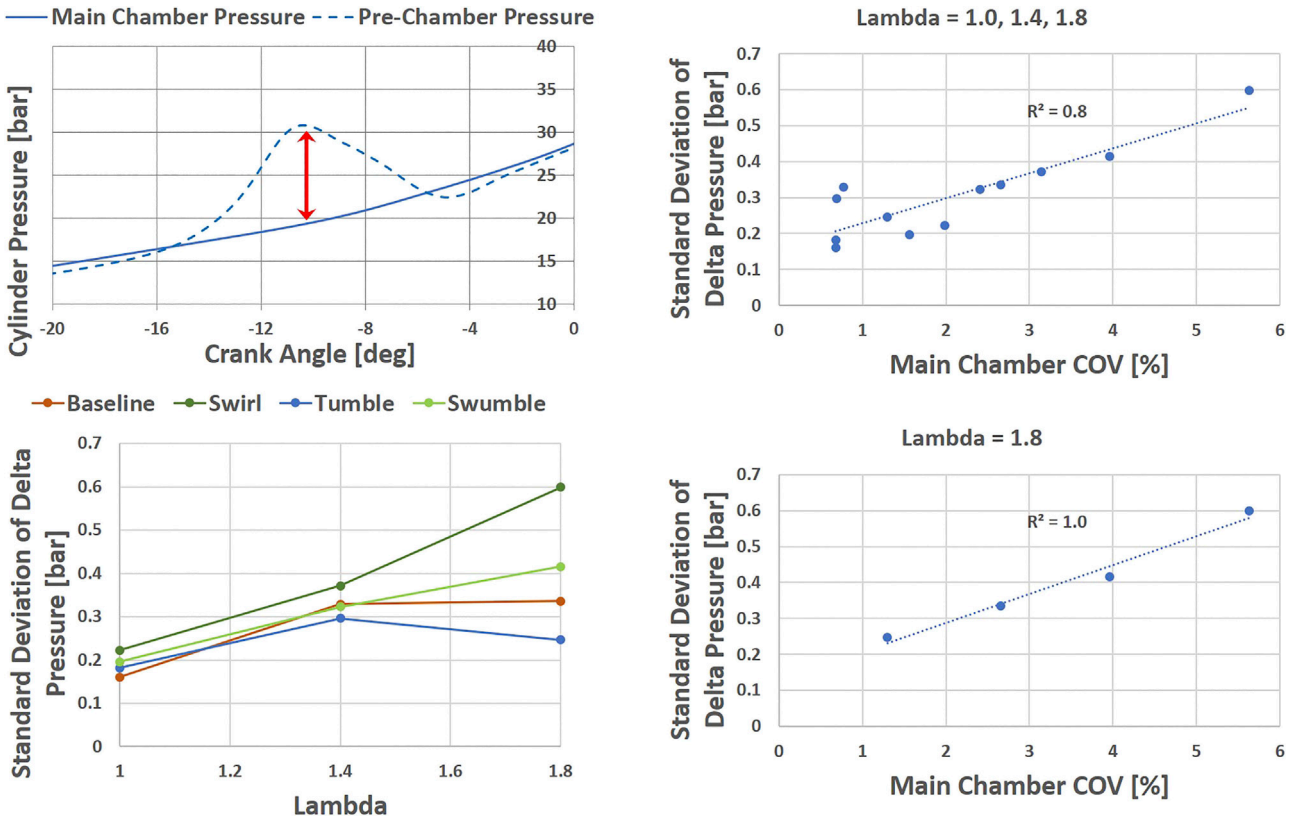

FIGURE 9 | Pre-chamber combustion metrics: illustration of chamber delta pressure **(top left)**; standard deviation of delta pressure vs. lambda **(bottom left)**; standard deviation of delta pressure vs. main chamber COV for lambda = 1.0–1.8 **(top right)**; standard deviation of delta pressure vs. main chamber COV for lambda = 1.8 **(bottom right)**.

previously, with parity at the lambda = 1 condition and an ever increasing disparity as the engine is enleaned. At the leanest condition considered in this dataset, lambda = 1.8, the tumble variant shows the least variation in chamber delta pressure and therefore the lowest main chamber COV, followed closely by the baseline variant. The swumble and swirl variants exhibited the highest degree of variation in chamber delta pressure.

Knock Limited Operation

With non-knock limited charge motion performance established, the engine was tested at condition 2 (3,000 rpm, 13.5 bar IMEPg), where knock is encountered over a large portion of the lambda sweep. IMEPg was selected as the constant load parameter in order to eliminate the influence of pumping losses at this highly boosted condition. The CA50 result in **Figure 10** shows that all charge motion variants require retarded combustion phasing to avoid knock over some portion of the lambda sweep. The swirl and swumble variants are knock limited over the entirety of the lambda sweep, while the baseline and tumble variants are fully free of knock at lambda values from approximately 1.7. As a result of this variable knock performance among the charge motion variants, the burn duration trends across the lambda sweep differ from the trends observed at the non-knock limited condition. At this condition, the largest discrepancy in burn duration occurs in the near-lean lambda range of 1.2–1.4. The variants with the most retarded combustion phasing, swirl and swumble, exhibit the shortest late burning duration (CA50-90) in this near-lean range due to the lower background cylinder pressure associated with retarded phasing. This trend becomes less prominent at lambda values beyond the near-lean region as bulk burn durations increase due to the engine's increasing performance sensitivity to lambda. At these ultra-lean conditions (lambda > 1.6) the tumble variant displays the fastest relative burn duration.

Because of the relatively high combustion efficiency in the near-lean region, the burn duration discrepancies in this region do not translate to any significant combustion efficiency disparities. Instead the trend appears similar to that of the non-knock limited condition, with the tumble variant producing clearly higher combustion efficiency in the ultra-lean region (**Figure 11**). This figure also displays ITE and BTE trends, the former providing the more accurate comparison at this condition because IMEPg is held constant. The swirl and swumble variants exhibit an ITE deficit compared to the others that tracks well with the differences in CA50. Once again, the tumble variant displays superior peak ITE and high sustained ITE in the ultra-lean region compared to the other variants.

Figure 11 also shows brake specific NO_x trends. The slightly lower NO_x emissions with the swirl and swumble variants from

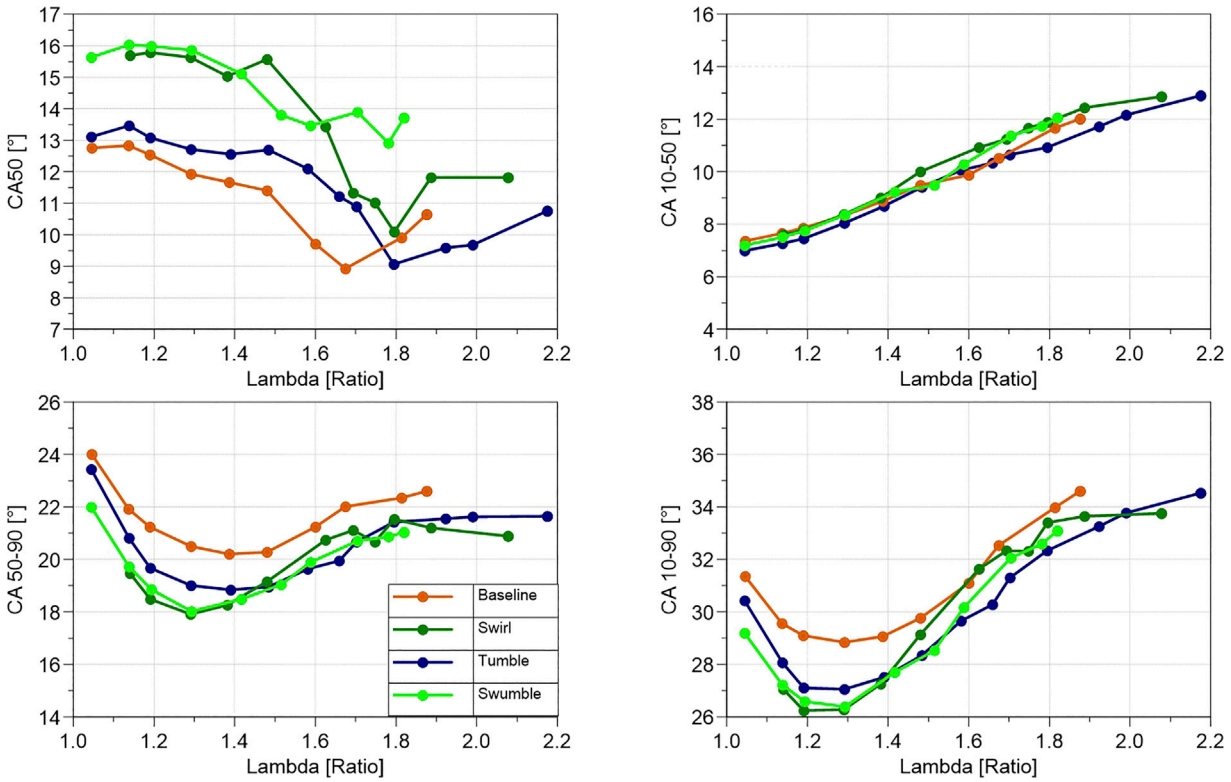

FIGURE 10 | Burn duration metrics vs. lambda; 3,000 rpm, 13.5 bar IMEPg.

lambda = 1.0 to at least lambda = 1.6 is reflective of the retarded combustion phasing required with these variants over this lambda range. Aside from the indirect effect of this knock sensitivity, it appears that charge motion does not have any significant impact on engine-out NO_x. This is consistent with the results at the non-knock limited condition.

Figure 12 demonstrates the advantage of the tumble variant across a sweep of load while lambda is held at a constant value of 1.65. A 1–3 percentage point advantage in combustion efficiency is present across the sweep from 6 to 15 bar IMEPg, without the severe deterioration at low loads exhibited by the swirl variant. This translates to a sustained advantage in ITE with the tumble variant across the load range.

CSSR Operation

For the CSSR condition 3 (1,500 rpm, 2 bar NMEP), a combustion stability limit of 0.4 standard deviation of NMEP is used, which is consistent with those of many production engines. **Figure 13** shows relative parity among the charge motion variants with the exception of the swumble variant, which exhibits a spark retard limit 10 crank angle degrees advanced from those of the other variants. This represents a significant reduction in spark retard capability for the swumble variant.

As is demonstrated in **Figure 13**, there is a disparity in combustion efficiency trends for the charge motion variants, with the tumble variant displaying consistently higher combustion efficiencies than the other variants. While this result has no detectable influence on specific exhaust enthalpy, it does correlate with the key emissions parameter of THC + NO_x, the emissions parameter of most interest in developing CSSR calibrations. THC emissions trends on their own generally mirror those of combustion efficiency. At a common CA50 of 50° after TDC, the tumble variant has a combined THC + NO_x level half of that of the swumble variant.

DISCUSSION

From the results presented in the previous section, one conclusion is clear: jet ignition engine performance can be optimized through the addition of tumble motion. The differences in key combustion parameters such as burn duration and knock mitigation are relatively muted at stoichiometric lambda values. The disparities increase progressively with increasing levels of dilution. The clearest example of this in all test conditions attempted is the consistent combustion efficiency trend. While all variants experience the expected deterioration in combustion efficiency as the engine is enleaned, the tumble variant exhibits deterioration at a lesser rate than all other variants. The swirl and swumble variants exhibit the most rapid deterioration.

Results from the CSSR test condition show an equivalent combustion efficiency trend not with lambda but with spark

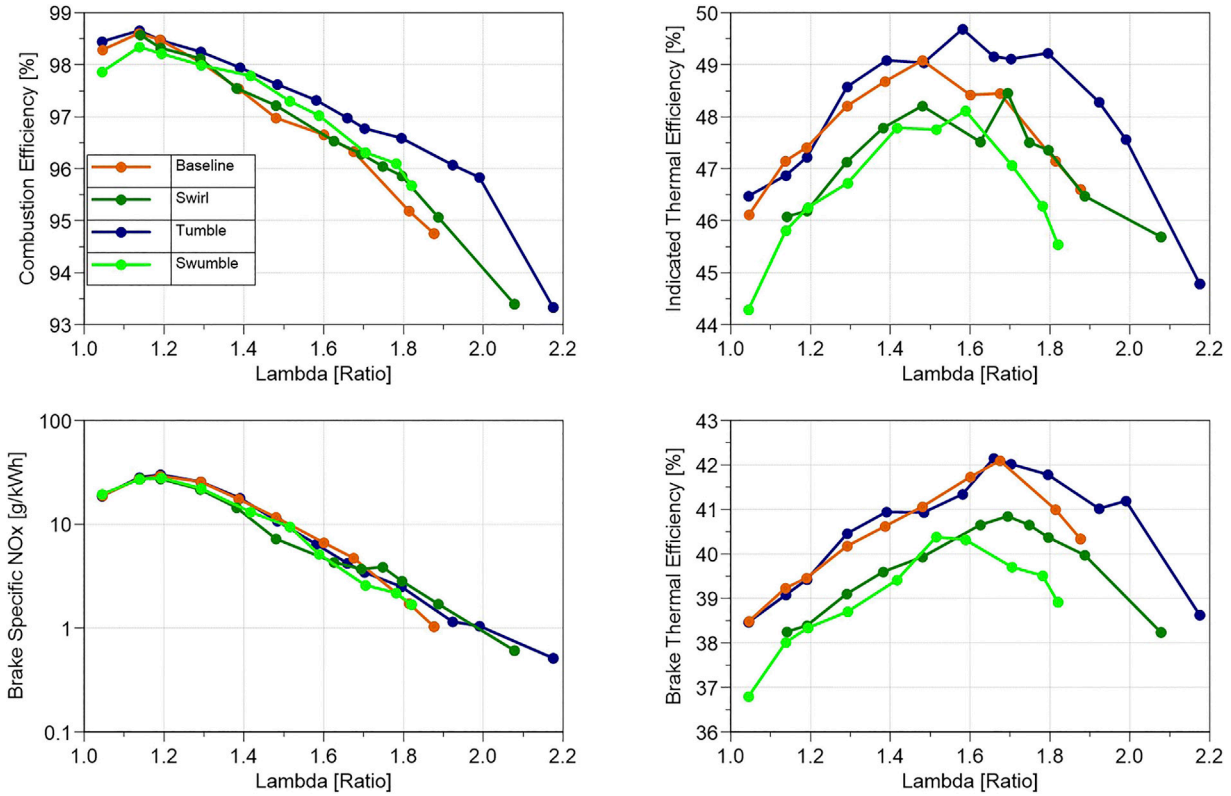

FIGURE 11 | Efficiency and emissions metrics vs. lambda; 3,000 rpm, 13.5 bar IMEPg.

retard. At this condition, the combustion efficiency disparity among the charge motion variants increases with increasing spark retard. Harmonizing this result with that of the lambda sweep tests, it is evident that tumble motion is most advantageous under low ignitability conditions, such as enleanment or heavy spark retard. Burn duration and emissions results support this conclusion, with the tumble variant promoting more rapid main chamber combustion and reduced incomplete combustion products.

The results therefore indicate that the TKE generated by the tumble variant promotes faster flame speeds in the main chamber that compensate for the slower tendency of flames in a cold, highly dilute combustion environment and in a low background pressure combustion environment. The latter point is supported by the combustion efficiency trend across the load sweep at a common lean lambda, whereby the combustion efficiency produced by the tumble variant did not degrade at lower loads to the same degree as the other variants. A potential alternative or supplementary effect to this is a potential charge motion impact on pre-chamber air mass at time of spark. Though fuel mass in the pre-chamber can be modulated independently through the pre-chamber fuel injector, air mass cannot be modulated directly, and so any charge motion-related impact on the pre-chamber filling process may impact the subsequent combustion events. This alternative hypothesis will be explored through future simulation.

Swirl appears largely detrimental to main chamber combustion under low ignitability conditions such as high levels of dilution. This could be indicative of the swirl boundary layer serving to accelerate heat loss from the lean flame to the cylinder walls, as opposed to tumble which produces high levels of TKE which can also extract heat from the system but in non-uniform ways. Lean flame front propagation is substantially reliant on preserving temperature to maintain the fuel chemical reaction kinetics. Robbing the process of heat could arrest certain areas of lean flame propagation. The combustion efficiency trends coupled with the efficiency loss analysis confirm that while increased tumble can produce slightly higher in-cylinder heat losses than the baseline, the introduction of swirl produces a more substantial increase in these losses.

The swirl and swumble variants consistently produce the least optimum results. While the swumble variant provides the same relative increase in tumble motion over the baseline as the tumble variant, the poor results indicate that the suboptimal effect of swirl motion under low ignitability conditions outweighs the benefits of the tumble ratio addition in this case.

Analysis of high speed pressure in the pre-chamber demonstrates that tumble produces a more stable pre-chamber combustion event, with the standard deviation of chamber delta pressure as an accurate surrogate for stability. The relative

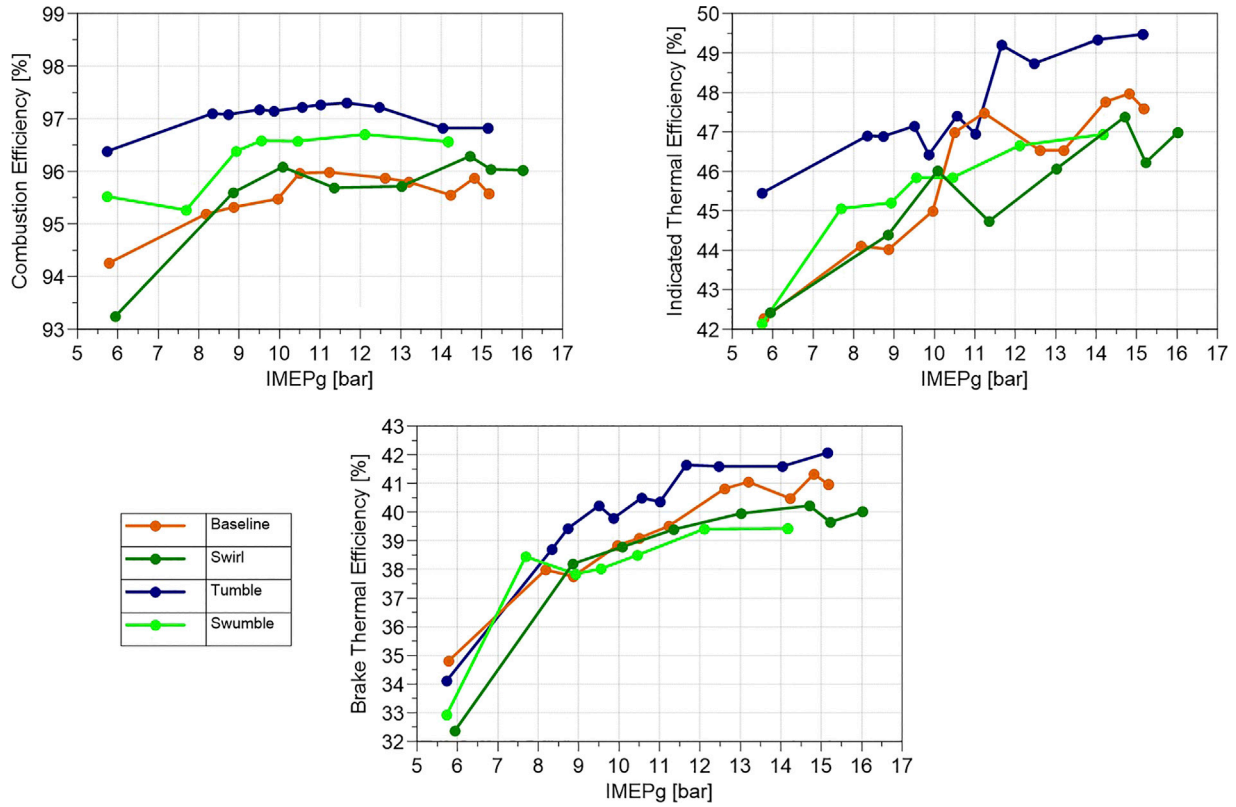

FIGURE 12 | Efficiency metrics vs. IMEPg; 3,000 rpm, lambda = 1.65.

stability of the pre-chamber combustion event influences the main chamber COV to a high degree, thereby impacting combustion efficiency at lean conditions and contributing to the lean limit determination. Simulation is needed to understand the mechanism behind this enhanced pre-chamber combustion stability with tumble, and conversely poor stability with swirl, since the main chamber charge motion direction likely does not translate directly to the pre-chamber. Possible sensitivities could include the impact of charge motion on fuel and air mass entering the pre-chamber during the compression stroke, effectiveness of scavenging during the intake stroke, and pre-chamber combustion duration.

While a high degree of tumble motion can detrimentally affect spark kernel formation under highly dilute conditions, the pre-chamber in the jet ignition engine effectively shrouds the spark plug and largely reorders the bulk charge motion as contents are forced through the nozzle orifices during the compression stroke. Therefore, pre-chamber jet ignition engines may be uniquely suited to a high degree of intake-based tumble motion that does not overly compromise volumetric efficiency by restricting the intake port. With the TKE addition being the most beneficial aspect of tumble, there may be other less intrusive methods (from a volumetric efficiency perspective) to generate TKE during the combustion process through combustion chamber, valve, or piston component design rather than relying solely on intake port design.

While the jet ignition engine is capable of tolerating a wide range of charge motion levels and types, tumble motion provides the most positive impact on performance. For the relatively modest 13% increase in tumble motion presented in this study, the jet ignition engine produced increases in peak gross ITE of 0.5–1 percentage point and increases in BTE of 0.5 percentage point, and the lambda corresponding to the peak efficiency point was shifted leaner by 0.2–0.3 lambda at some conditions. The shift to leaner peak efficiency lambdas, coupled with the generally higher combustion efficiencies with the tumble variant allow the engine to operate at a higher efficiency with lower engine-out NO_x, CO, and potentially THC emissions.

This study examined several specific charge motion types and levels, but a parametric sweep is needed to determine true optimums. This optimal level will likely be specific to engine intake port, combustion chamber, and pre-chamber geometry. Higher levels of tumble for instance will present volumetric efficiency trade-offs in intake port design and in-cylinder heat loss trade-offs that can be impacted by both combustion chamber and pre-chamber geometry. The results of this study provide indicative trends for charge motion-based optimization and present approximate magnitudes of the stability, burn rate, and efficiency benefits that can be realized.

With the introduction of a secondary fueling source and strategy, and lambda as a wide-ranged variable, active jet ignition engines offer many optimization pathways. Charge

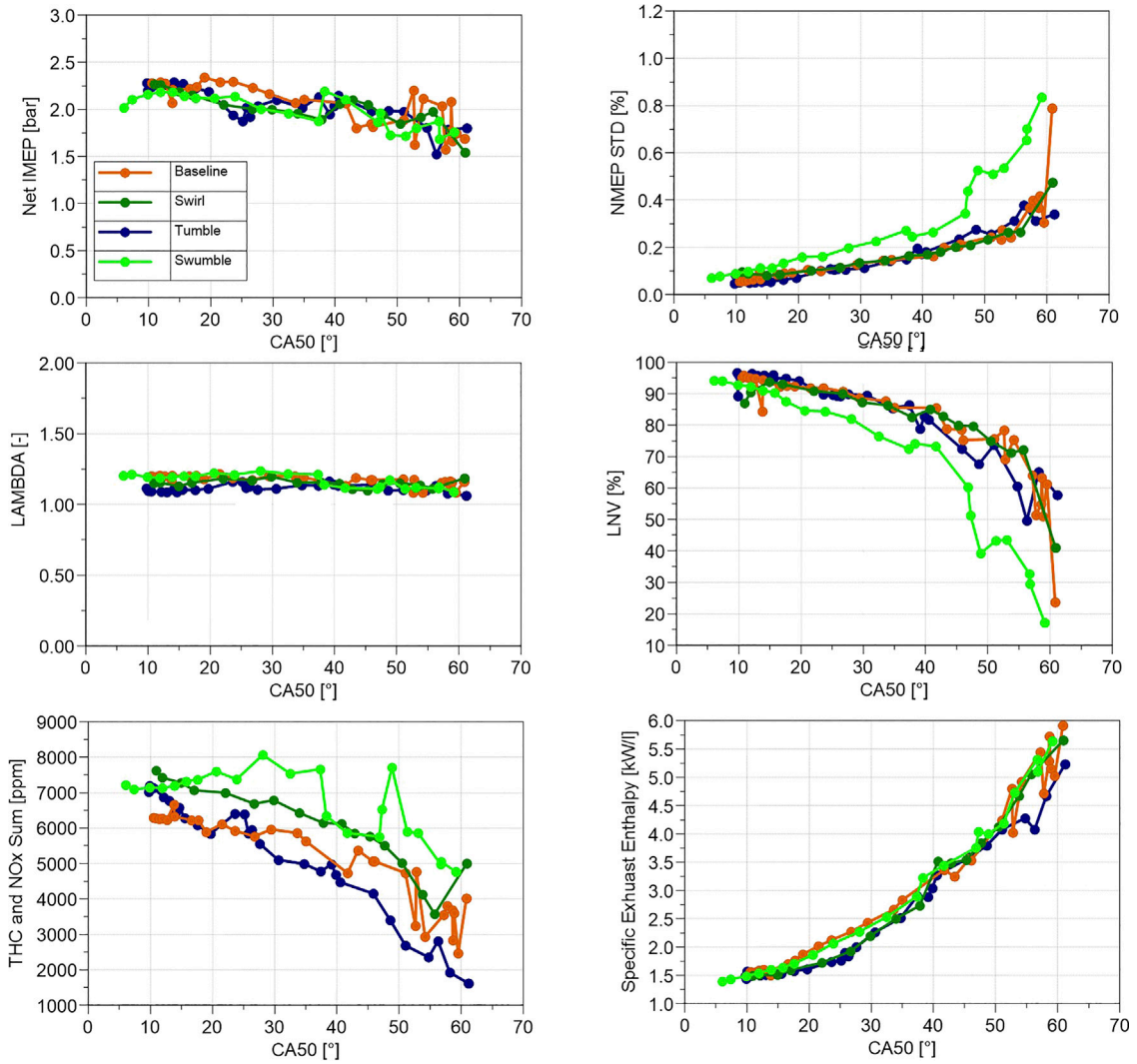

FIGURE 13 | Combustion stability, emissions, and exhaust enthalpy metrics vs. lambda; 1,500 rpm, 2 bar NMEP, 25°C fluids.

motion has historically been an underexplored pathway. This study aims to increase the current understanding of the influence of charge motion on the jet ignition combustion process and provides a roadmap for jet ignition engine optimization.

Further work will include further analysis of combustion data in the pre-chamber to understand the effect that varying charge motion level and type have on pre-chamber combustion. The engine test data will also be matched against 3D analysis results to establish correlation and to understand the impact that charge motion has on in-pre-chamber mixture preparation, including how charge motion near the nozzle orifices impacts pre-chamber filling and in-pre-chamber motion during the compression stroke. The 3D analysis will also analyze whether or not charge motion has an impact on relative ignition site location and early flame front formation in the main chamber. Potential future studies could also include a detailed analysis of in-pre-chamber emissions formation sensitivity to charge motion. Finally, an aspect of these results that is not explored here is whether pre-chamber geometry can be adapted for specific charge motion types. If so, this could be useful in applications where the pre-chamber must be adapted to an existing engine with little to no ability to adjust existing charge motion, such as in heavy duty diesel engine conversions to spark ignited operation. The results of this study may help lay the initial groundwork for such future studies.

DATA AVAILABILITY STATEMENT

The datasets presented in this article are not readily available because the data was generated through funding provided by MAHLE Powertrain. Requests to access the datasets should be directed to powertrain@mahle.com.

AUTHOR CONTRIBUTIONS

The manuscript was written through contributions of all authors. All authors have given approval to the final version of the manuscript. Specifically, the study was performed by MB, NP, and SS, with AC and HB providing guidance.

FUNDING

The authors declare that this study received funding from MAHLE Powertrain. The funder was not involved in the study design, collection, analysis, interpretation of data, the writing of this article or the decision to submit it for publication.

REFERENCES

Attard, W., Toulson, E., Fraser, E., and Parsons, P. (2010). A turbulent jet ignition pre-chamber combustion system for large fuel economy improvements in a modern vehicle powertrain. SAE, Technical Paper 2010-01-1457. doi:10.4271/2010-01-1457

Bassett, M., Hall, J., Cains, T., Underwood, M., Wall, R., and Richards, B. G. R. (2017). Dynamic downsizing gasoline demonstrator. *SAE Int. J. Engines* 10 (3), 884–891. doi:10.4271/2017-01-0646

Biswas, S., Tanvir, S., Wang, H., and Qiao, L. (2016). On ignition mechanisms of premixed CH_4/air and H_2/air using a hot turbulent jet generated by pre-chamber combustion. *Appl. Therm. Eng.* 106, 925–937. doi:10.1016/j.applthermaleng.2016.06.070

Bozza, F., De Bellis, V., Berni, F., D'Adamo, A., and Maresca, L. (2018). Refinement of a 0D turbulence model to predict tumble and turbulent intensity in SI engines. Part I: 3D analyses. SAE, Technical Paper 2018-01-0850. doi:10.4271/2018-01-0850

Bunce, M., Blaxill, H., Kulatilaka, W., and Jiang, N. (2014). The effects of turbulent jet characteristics on engine performance using a pre-chamber combustor. SAE, Technical Paper 2014-01-1195. doi:10.4271/2014-01-1195

Bunce, M., and Blaxill, H. (2016). Sub-200 g/kWh BSFC on a light duty gasoline engine. SAE, Technical Paper 2016-01-0709. doi:10.4271/2016-01-0709

Bunce, M., and Blaxill, H. (2018). *Internal combustion engine*. U.S. Patent No. 10,458, 311.

Bunce, M., Peters, N., Subramanyam, S. K. P., and Blaxill, H. (2019). "Assessing the low load challenge for jet ignition engine operation," in Proceedings of the institute of mechanical engineers internal combustion engines conference December 11-12, 2019, Birmingham, UK. CRC Press.

Bureshaid, K., Feng, D., Zhao, H., and Bunce, M. (2019). Combustion and emissions of gasoline, anhydrous ethanol, and wet ethanol in an optical engine with a turbulent jet ignition system. *Proc. Inst. Mech. Eng., Part D* 233 (13), 3528–3537. doi:10.1177/0954407019825999

Chinnathambi, P., Bunce, M., and Cruff, L. (2015). RANS based multidimensional modeling of an ultra-lean burn pre-chamber combustion system with auxiliary liquid gasoline injection. SAE, Technical Paper 2015-01-0386. doi:10.4271/2015-01-0386

Dale, J., and Oppenheim, A. (1981). Enhanced ignition for I.C. Engines with premixed gases. SAE, Transactions Paper 810146, Vol. 90.

Germane, G., Wood, C., and Hess, C. (1983). Lean combustion in spark-ignited internal combustion engines—a review. SAE, Technical Paper 831694.

Gussak, L. A., Karpov, V. P., and Tikhonov, Y. V. (1979). The application of lag-process in prechamber engines. SAE, Technical Paper 790692. doi:10.4271/790692

Heywood, J. (1988). *Internal combustion engine fundamentals*. New York: McGraw-Hill.

Hill, P. G., and Zhang, D. (1994). The effects of swirl and tumble on combustion in spark-ignition engines. *Prog. Energy Combust. Sci.* 20, 373–429. doi:10.1016/0360-1285(94)90010-8

Husted, H., Piock, W., and Ramsay, G. (2009). Fuel efficiency improvements from lean stratified combustion with a solenoid injector. SAE, Technical Paper 2009-01-1485.

Loeper, P., Ra, Y., Foster, D., and Ghandhi, J. (2014). Experimental and computational assessment of inlet swirl effects on a gasoline compression ignition (GCI) light-duty diesel engine. SAE, Technical Paper 2014-01-1299. doi:10.4271/2014-01-1299

Mastorakos, E., Allison, P., Giusti, A., De Oliveira, P., Benekos, S., Wright, Y., et al. (2017). Fundamental aspects of jet ignition for natural gas engines. *SAE Int. J. Engines* 10 (5), 2429–2438. doi:10.4271/2017-24-0097

Murase, E., and Hanada, K. (2000). Enhancement of combustion by injection of radicals. SAE, Technical Paper 2000-01-0194. doi:10.4271/2000-01-0194

Patrie, M., Martin, J., and Engman, T. (1998). Inlet port geometry and flame position, flame stability, and emissions in an SI homogeneous charge engine. SAE, Technical Paper 982056. doi:10.4271/982056

Peters, B., and Quader, A. (1978). "Wetting" the appetite of spark ignition engines for lean combustion. SAE, Technical Paper 780234. doi:10.4271/780234

Peters, N., Krishna Pothuraju Subramanyam, S., Bunce, M., Blaxill, H., and Cooper, A. (2020). Optimization of lambda across the engine map for the purpose of maximizing thermal efficiency of a jet ignition engine. *SAE Int. J. Adv. Curr. Prac. Mobility* 2 (6), 3140–3150. doi:10.4271/2020-01-0278

Qi, Y., Ge, X., and Dong, L. (2015). Numerical simulation and experimental verification of gasoline intake port design. SAE, Technical Paper 2015-01-0379. doi:10.4271/2015-01-0379

Quader, A. A. (1974). Lean combustion and the misfire limit in spark ignition engines. SAE, Technical Paper 74105. doi:10.4271/741055

Ruhland, H., Lorenz, T., Dunstheimer, J., Breuer, A., and Khosravi, M. (2017). A study on charge motion requirements for a class-leading GTDI engine. SAE, Technical Paper 2017-24-0065. doi:10.4271/2017-24-0065

Sens, M., Binder, E., Reinicke, P.-B., Riess, M., Stappenbeck, T., and Woebke, M. (2018). "Pre-chamber ignition and promising complementary technologies," in 27th Aachen colloquium automobile and engine technology, Aachen 2018 Oct, 957-998. doi:10.4271/2018-37-0003

Solomon, A., and Szekely, G. (2003). Combustion characteristics of a reverse-tumble wall-controlled direct-injection stratified-charge engine. SAE, Technical Paper 2003-01-0543. doi:10.4271/2003-01-0543

Toulson, E., Schock, H., and Attard, W. (2010). A review of pre-chamber initiated jet ignition combustion systems. SAE, Technical Paper 2010-01-2263. doi:10.4271/2010-01-2263

Urushihara, T., Nakada, T., Kakuhou, A., and Takagi, Y. (1996). Effects of swirl/tumble motion on in-cylinder mixture formation in a lean-burn engine. SAE, Technical Paper 961994. doi:10.4271/961994

Vedula, R., Song, R., Stuecken, T., Zhu, G., and Shock, H. (2017). Thermal efficiency of a dual-mode turbulent jet ignition engine under lean and near-stoichiometric operation. *Int. J. Engine Res.* 18 (10), 1055–1066. doi:10.1177/1468087417699979

Wakai, K., Kito, S., and Sumida, I. (1993). Effect of small hydrogen jet flame on augmentation of lean combustion. SAE, Technical Paper 931943. doi:10.4271/931943

Yamamoto, H. (1999). Investigation on relationship between thermal efficiency and NOx formation in ultra-lean combustion. SAE Journal Paper JSAE 9938083. Society of Automotive Engineers.

Conflict of Interest: Authors MB, SKPS, NP and HB were employed by MAHLE Powertrain LLC. The authors declare that this study received funding from MAHLE Powertrain LLC. The funder was not involved in the study design, collection, analysis, interpretation of data, the writing of this article or the decision to submit it for publication.